Ultrasonics 121 (2022) 106684

Contents lists available at ScienceDirect

Ultrasonics

journal homepage: www.elsevier.com/locate/ultras

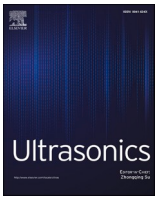

Microstructure and mechanical properties of dissimilar NiTi and 304 stainless steel joints produced by ultrasonic welding

S.S. Ao [a], M.P. Cheng [a], W. Zhang [b,*], J.P. Oliveira [c], S.M. Manladan [a], Z. Zeng [d], Z. Luo [a]

[a] School of Material Science and Engineering, Tianjin University, Tianjin 300072, China
[b] Advanced Production Engineering, Engineering and Technology Institute Groningen, Faculty of Science and Engineering, University of Groningen, 9747 AG, the Netherlands
[c] UNIDEMI, Department of Mechanical and Industrial Engineering, NOVA School of Science and Technology, NOVA University Lisbon, 2829-516 Caparica, Portugal
[d] School of Mechanical and Electrical Engineering, University of Electronic Science and Technology of China, Sichuan 611731, China

ARTICLE INFO

Keywords:
NiTi alloys
304 stainless steel
Ultrasonic spot welding
Intermetallic compounds
Interlayer

ABSTRACT

Superelastic NiTi alloy and 304 stainless steel (304 SS) were joined with a Cu interlayer by ultrasonic spot welding (USW) using different welding energy inputs. The surface morphology, interfacial microstructure, mechanical properties, and fracture mechanisms of the dissimilar NiTi/304 SS USWed joints were studied. The results showed that the surface oxidation intensified with increasing ultrasonic welding energy due to mutual rubbing between tools and sheets. The weld interface microstructure exhibited voids or unbonded zones at low energy inputs, while an intimate contact was established at the joining interface when applying a higher energy input of 750 J. With increasing energy input to 750 J, the weld interface shows two interfaces due to the behavior of plastic flow of Cu interlayer. The lap-shear load of the joints first increased, achieving a maximum value of ~690 N at an energy input of 750 J, and then decreased with further increase in welding energy. Interfacial failure was observed at NiTi/Cu interface at all energy inputs, and no intermetallic compounds were found on the fracture surfaces of both the NiTi/Cu and Cu/304 SS interfaces.

1. Introduction

During the last few decades, NiTi shape memory alloys have received extensive attention due to their unique functional properties (shape memory effect (SME) and superelasticity (SE)), excellent mechanical properties, high corrosion resistance, and good biocompatibility. They have been widely used in the automotive, aerospace, microelectronics, civil engineering and biomedical fields [1,2]. However, with the advancement in science and technology, NiTi-based alloys are required to exhibit superior performance to meet the more demanding requirements. Consequently, it is difficult for a single monolithic NiTi structure to meet the performance requirements for different parts of a product at the same time. Also, the high cost of NiTi alloys greatly limits their scope of application. Therefore, joining NiTi alloys to other dissimilar materials is an effective way to overcome these challenges and exploit the advantages of different materials for the products. As a low cost material, stainless steels (SS) also possess excellent corrosion resistance and biocompatibility, which have been employed as an important structural material in several fields for decades [3].

As a result, the components with NiTi and SS dissimilar joints often possess the inherent advantages of a good combination of both functional, structural properties and lower cost. For instance, composite orthodontic wires and medical occluders can be made from NiTi and SS through the welding process, thereby combining the super-elasticity and rigidty of these alloys [4,5]. It has also been reported that a composite torsional actuator made of NiTi alloy and 304 SS tubes would increase the system integrity [6,7]. However, several challenges were encountered when joining these two dissimilar alloys together due to the significant differences in their physical and chemical properties. NiTi alloys, sensitive to temperature changes, exhibit poor weldability, and the deterioration of the SME and SE makes the welding process even more challenging [8,9].

In recent years, attempts have been made to develop reliable processes for joining NiTi to SS. Fusion-based welding processes, including laser welding [10–16], TIG [7,17], plasma welding [18], and resistance welding [19] were employed to join NiTi to 304 SS. It was revealed that

* Corresponding author.
E-mail addresses: ao33@tju.edu.cn (S.S. Ao), 2019208169@tju.edu.cn (M.P. Cheng), wei.zhang@rug.nl (W. Zhang), jp.oliveira@fct.unl.pt (J.P. Oliveira), smmanladan.mec@buk.edu.ng (S.M. Manladan), zhizeng@uestc.edu.cn (Z. Zeng), lz_tju@163.com (Z. Luo).

https://doi.org/10.1016/j.ultras.2022.106684
Received 28 March 2021; Received in revised form 11 December 2021; Accepted 6 January 2022
Available online 10 January 2022

Table 1
Chemical composition of the materials used in this study (wt%).

Material	Ni	Ti	Cu	Fe	Cr	Mn	Si	C + S + P
NiTi	55.87	44.13	–	–	–	–		
304 SS	9.40	–	–	70.10	18.40	1.40	0.63	0.06
Cu	–	–	99.99	–	–	–	–	–

traditional fusion welding processes would result in the formation of brittle intermetallic compounds (IMCs) in the welds, such as $TiFe_2$, $TiCr_2$, deteriorating the mechanical properties of the joints [8,16]. Because of this, filler metals have been used to restrict the formation of brittle IMCs in traditional fusion welding processes. For example, a Ni filler metal was found to effectively restrain the formation of the brittle $TiFe_2$ phase and increase the amount of ductile γ-Fe phases instead, thereby improving greatly the performance of joints [6,7,10]. According to Asadi et al. [5], joints with more homogenous weld composition would be obtained when Ni powder was used as filler metal. However, the weld configuration using the filler metals during the fusion welding processes is more complicated, which limits its application in industry.

Recently, solid-state welding processes have been shown to be suitable for jointing NiTi alloy to SS, as no solid-liquid-solid phase transition will occur. Belyaev et al. [20] used explosion welding to fabricate NiTi-SS joints and obtained good joints without any defects or IMCs. However, the phase transformation was suppressed due to the impact loading. Friction welding was also employed to join NiTi-SS dissimilar alloys with/without a Ni interlayer [21]. Brittle $TiFe_2$ and $TiCr_2$ IMCs were generated when no interlayer was used. With the Ni interlayer, the brittle phases were converted into ductile γ-Fe phases and Ni_3Ti phases, thereby improving the joint mechanical performance. Other processes, such as laser brazing [9] and impact butt welding [22] were also used. However, the inevitable grain coarsening in the NiTi heat affected zone could reduce the superelasticity of the joints.

As a promising solid-state joining method, ultrasonic spot welding (USW) is a process in which ultrasonic energy, combined with moderate clamping pressure and amplitude, is transmitted to the materials through the sonotrode to produce solid-state bonding. USW is a reliable technique for dissimilar materials joining, in which the formation of brittle IMCs commonly formed in fusion welding process can be avoided. The process also possesses many other advantages such as low energy consumption and ease of operation [23–25]. Moreover, USW has been proved as a reliable welding method to join NiTi alloys using soft metal interlayers, such as copper. The soft behavior of the interlayer can effectively accommodate the high strain imposed during the USW process. Thus, adding an interlayer with higher plasticity can alleviate the local stress concentration generated during welding process, and produce severe plastic deformation near the bonding interface to obtain a well-bonded joint. Cu is a soft metal with lower hardness than NiTi and SS. As such, it is easy to induce plastic deformation and promote bonding with the base metals during the USW process. Furthermore, no brittle IMCs would be formed between Cu and NiTi/SS interfaces during the USW process according to the literature [14]. Zhang et al. [26–28] reported that a Cu interlayer could improve the bonding strength of similar NiTi USWed joints due to the increase of the friction coefficient and the compensation of the thermal stresses generated during USW. In addition, brittle IMCs were not observed at the joining interfaces during USW process with the addition of Cu interlayer. Therefore, to develop a reliable method of joining NiTi/SS for potential practical applications, a Cu interlayer can be promising solution via USW.

To the best of the author's knowledge, there are no reports on the weldability and mechanical behavior of dissimilar NiTi/SS USW joints with Cu interlayer yet. To develop a reliable method of joining NiTi/SS for potential practical applications, a detailed investigation on the joining of dissimilar NiTi and SS with Cu interlayer by USW is carried out in this present work.

Table 2
Mechanical properties of the materials at the room temperature.

Material	Yield strength (MPa)	Tensile strength (MPa)	Hardness (HV0.2)
NiTi	517	707	245
304 SS	269	705	190

2. Experimental

2.1. Materials and methods

Superelastic NiTi shape memory alloy (fully austenitic at room temperature) and commercial AISI 304 SS sheets (γ-Fe) with both dimensions of 60 mm × 15 mm × 0.15 mm were used as the base materials (BM). A 20 μm-thick pure Cu foil with dimensions of 15 mm × 15 mm was used as an interlayer to improve the joint performance. The chemical compositions and mechanical properties of the BM are listed in Table 1 and Table 2, respectively. The as-received NiTi alloy sheets were subjected to cold rolling, followed by stress relief annealing. Before welding, NiTi alloy specimens were immersed in a solution of 7.5% HF, 20% HNO_3 and 72.5% H_2O (in volume) for one minute to remove the oxide layer, and finally cleaned with alcohol and dried.

The welding workpieces were assembled with an overlapping of 15 mm, and the Cu interlayer was placed between the NiTi and SS sheets, as schematically illustrated in Fig. 1. During USW, the interfacial temperature was measured using a type-K thermocouple of 0.08 mm in diameter embedded in the weld center of the interfaces. Although the thermocouple was subjected to the severe plastic deformation and ruptured sometimes, the real thermal history in weld region would be detected. To properly determine the temperature at the interface during the USW process, the average interfacial temperature values were obtained from five specimens conducted at each welding energy. A SONICS ultrasonic welding system (MSC4000-20), shown in Fig. 2 (a), was used to produce the welds at the center of the overlap area. The welding system was operated at a frequency of 20 kHz. A normal clamping pressure of 0.4 MPa and vibration amplitude of 55 μm were used, while the input energy varied in the range of 500 J to 1000 J. The sonotrode horn was a square with 8 mm sides and the detailed dimensions of the sonotrode tip and anvil are shown in Fig. 2 (b)-(c). During the USW process, the vibration direction was parallel to the sheets rolling direction.

2.2. Microstructure characterization and mechanical testing

For microstructure characterization, the welding joints produced under 500, 750 and 1000 J were sectioned across their weld centerline along the vibration direction using wire electrical discharge machining, and then ground and polished according to standard metallography procedures. The surface morphology of the joints was observed with a digital microscope (VHX-2000C, KEYENCE, Osaka, Japan). The microstructures were characterized by a scanning electron microscope (SEM; SU1510, HITACHI, Tokyo, Japan) equipped with an energy dispersive spectrometer (EDS). Tensile-shear tests were conducted at room temperature using a Micro Tester 5848 (INSTRON, Norwood, America) at a constant displacement speed of 0.5 mm/min. The loading direction was set perpendicular to the vibration direction. Three samples were tested for each energy input to ensure statistical accuracy, and the mechanical

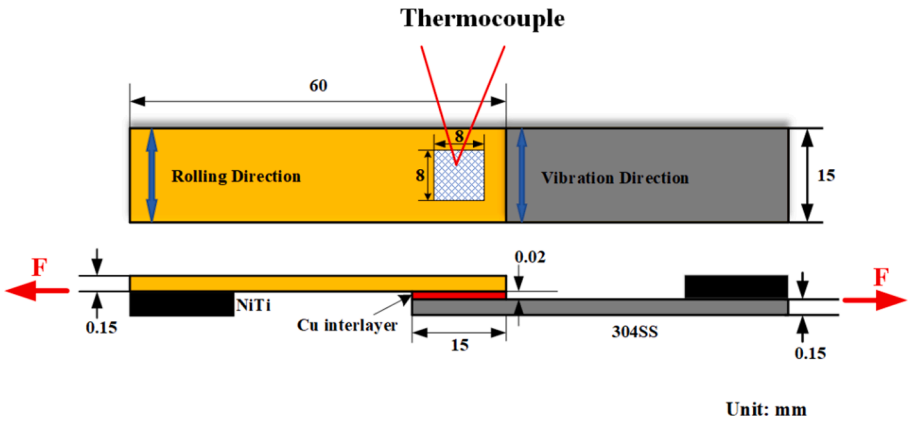

Fig. 1. Configuration of the weld coupon.

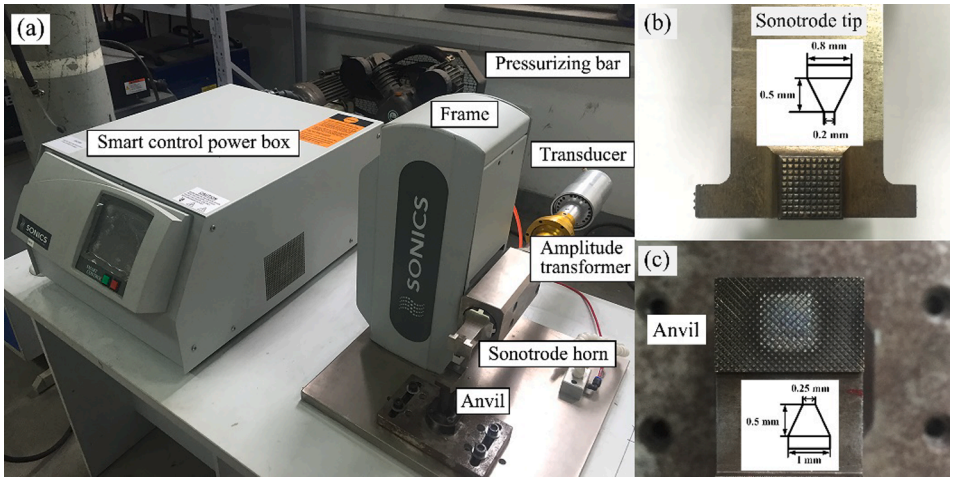

Fig. 2. Experimental setup: (a) Ultrasonic metal spot welding setup, (b) and (c) pattern and demensions of the sonotrode tip and anvil.

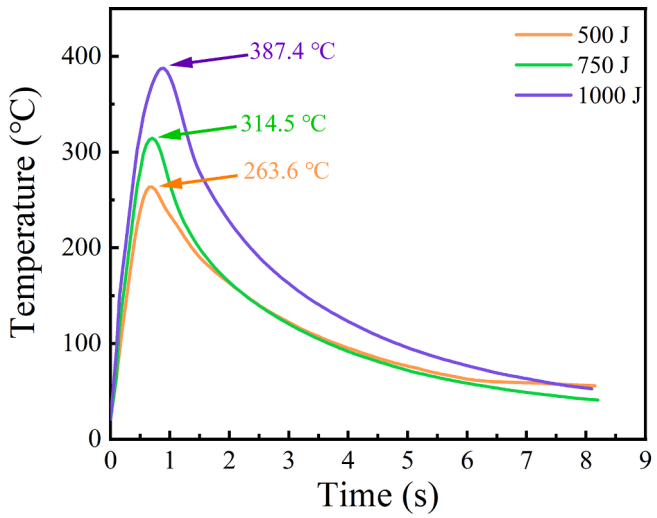

Fig. 3. Interfacial thermal profiles of weld coupons with different welding energy inputs.

performance was expressed as the average value of the failure loads. After the tensile test, the fracture surfaces were observed by digital microscope, SEM and EDS. To identify the phases generated during USW, X-ray diffraction analysis (XRD; D8 Advanced, BRUKER, Karlsruhe, Japan) was carried out on the fracture surfaces. The XRD analysis was performed at 40 kV and 40 mA with Cu-Kα radiation. The diffraction angle (2θ) ranged from 20° to 100° with a step size of 6°/min.

3. Results and discussion

3.1. Interfacial thermal cycles measurement

Fig. 3 shows the interfacial temperature profiles in the center of weld interfaces at various welding energy inputs. It is observed that the temperature increased rapidly from room temperature and reached a peak when the high power ultrasonic energy was applied to the weld zone. Then the interfacial temperature dropped rapidly due to the heat dissipation caused by the cooling gas. The measured peak temperature of 263.6 °C, 314.5 °C, 387.4 °C corresponding to the welding energy input of 500, 750 and 1000 J shows that more heat generated at the welding interfaces due to the increasing energy input. The welding peak temperatures did not reach half of the melting point of the BM (the melting points of NiTi, Cu, 304 SS are more than 1000 °C), indicating that welding occurred through a solid-state bonding process. During the USW process, friction heat was generated by the mutual rubbing between the interfaces, leading to material softening and severe plastic deformation. Generally, the high peak temperature promotes material softening and the decrease in yield strength of the materials. This is conducive to more severe plastic deformation of the materials, resulting in a robust interfacial bonding during welding. Eventually, the sound USWed joints with good joining strength can be obtained. However, it should be noted that excessive material thinning and cracks may occur

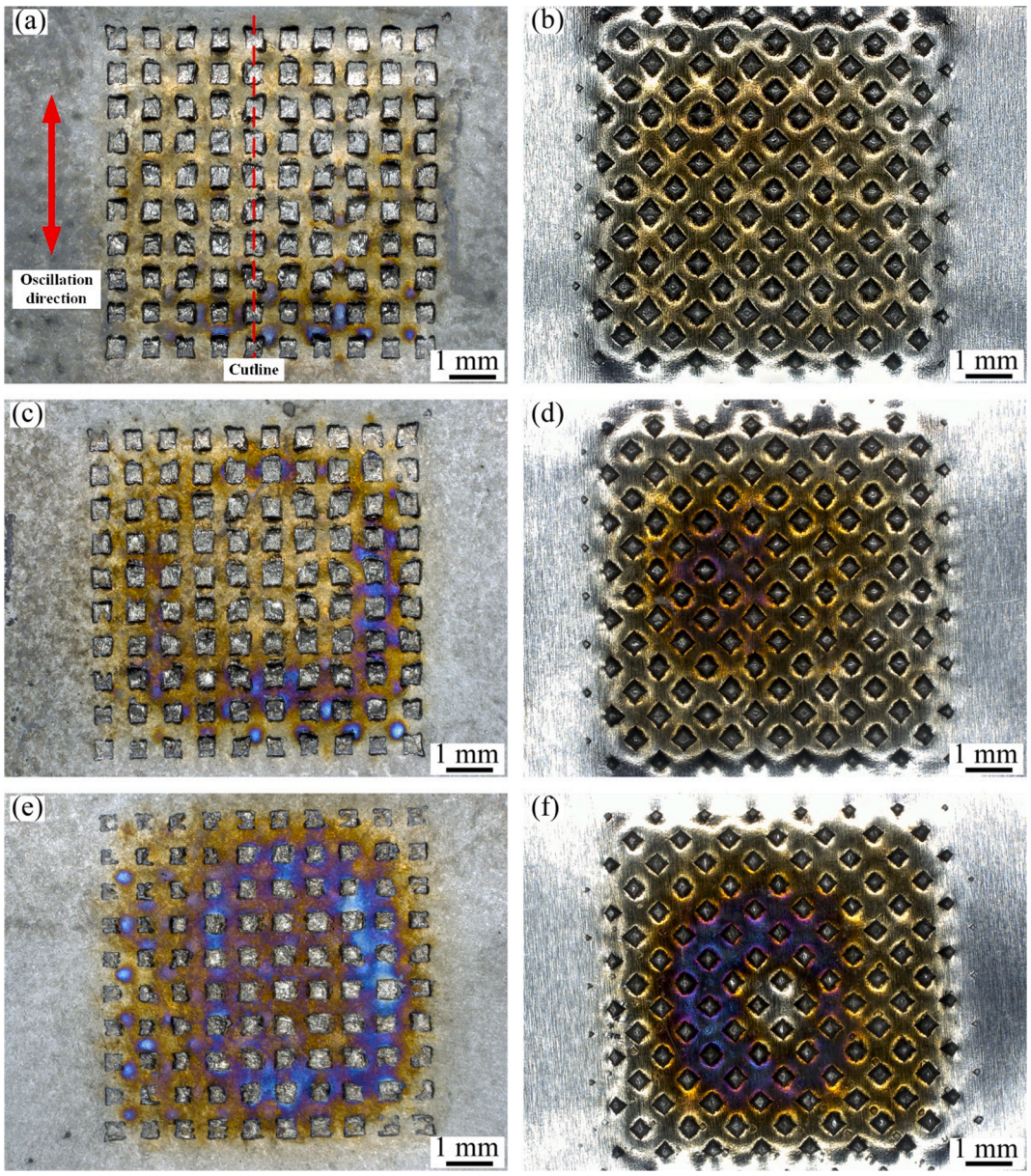

Fig. 4. Surface morphology of welded specimens at different welding energy: (a) and (b) top and bottom under 500 J, (c) and (d) 750 J, (e) and (f) 1000 J.

when the interfacial temperature exceeds a certain temperature threshold. Besides, high interfacial temperature during the USW process would cause severe surface oxidation of NiTi alloys due to its sensitivity to the temperature [2,8,9]. The surface oxidation and weld microstructure of joints under varying welding energy will be discussed in the following parts.

3.2. Surface morphology of welds

Typical surface morphologies of the welds at the sonotrode tip and anvil side are shown in Fig. 4. Referring to the figures, the imprints caused by the sontrode tip and anvil can be clearly seen on the surfaces of the specimens. The color of the surfaces appeared yellowish at low energy, which changed to violet with increasing energy input, mainly attributed to the fact that NiTi alloy and 304 SS are very sensitive to high temperature under atmospheric conditions [26]. During the welding process, the sonotrode exerted normal forces on the materials to clamp them, and then shear forces were exerted on the materials due to friction. The rapid sliding and friction between the sonotrode tip and the material surface would generate a large amount of heat on the material surface, giving rise to the surface oxidation. During the thermal circle history, complex multiple oxidation products were formed on the NiTi surface. Among them, the TiO_2 layer is usually formed first, which is the most thermodynamically favored oxide [29]. Similar surface oxidation color evolution has also been reported by Cisse et al. [30]. Furthermore, the NiTi side had more severe surface oxidation than the 304 SS side due to the higher temperature generated on the top surface. During the USW process, the sonotrode tip exerted a normal pressure to the top workpiece (NiTi side), which conducted the workpieces in motion with a certain vibration speed. And the bottom 304 SS was driven to move by the friction of the upper workpiece and the Cu interlayer, and its motion tended to lag behind the NiTi and Cu interlayer. Therefore, more slippage occurred between the sonotrode tip and NiTi due to the higher hardness of the NiTi alloy, resulting in a higher temperature being developed [31,32]. Plastic deformation would start from the material surface under the peaks of the sonotrode tip due to material softening, leading to the formation of imprints [33,34]. The surface oxidation became more severe with increasing energy input, which is in agreement

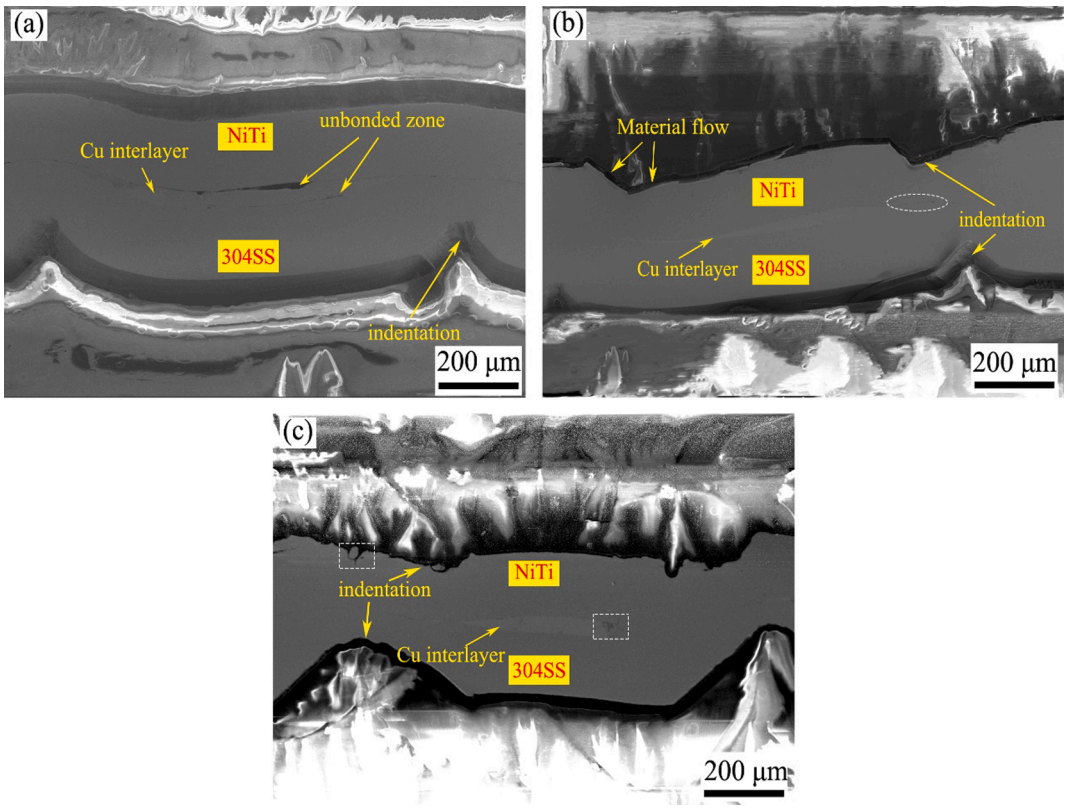

Fig. 5. SEM images of the cross-section of NiTi/304 SS joints with Cu interlayer produced at energy input of (a) 500 J, (b) 750 J, (c) 1000 J.

with the thermal history discussed earlier. These observations are consistent with previous studies [28,31]. It should be noted that the surface oxidation originated from the edge of the welded specimens due to the introduction of asymmetrical normal stresses during the USW process, which might be associated with the uneven abrasion on the surfaces of the sonotrode tip and anvil.

3.3. Weld interface microstructure

To futher understand the relationship between microstructure evolution and joint performance, microstructural analysis was performed at the faying interfaces of the joints. Fig. 5 shows the SEM images of the dissimilar joints at various welding energy inputs. Under the lower energy of 500 J, as shown in Fig. 5 (a), the indentation of the sonotrode tip on the NiTi surface is not obvious while the imprints on the 304 SS surface are clearly visible, which is mainly attributed to the higher hardness of NiTi, leading to more mutual slippage between the sontrode tip and NiTi surface rather than more penetration between the anvil knurls and 304 SS surface. Subsequently, the imprints of the sonotrode and anvil intensified with increasing energy input due to increasing plastic deformation and interfacial temperature. However, a high energy input of 1000 J would lead to significant materials thinning as well as extrusion of the BM between the knurls of sonotrode tip and anvil in the weld area, as shown in Fig. 5 (c), which will have a negative effect on the joint strength [35]. At low energy, bonding occurred first under the edges of the sonotrode tip. The weld interface remained macroscopically flat, whereas the weld join-line gradually developed a convoluted wave-like appearance with the increasing energy inputs. This could be explained by the higher pressure beneath the sonotrode tip ridges caused by the elastic deflection of the sheets as they were in intimate contact. Besides, several voids could be observed at the weld interface at an energy input of 500 J (Fig. 5 (a)), indicating that there was insufficient friction during welding. According to Lee et al. [33], a good quality weld in ultrasonic welding can be obtained when the materials interface

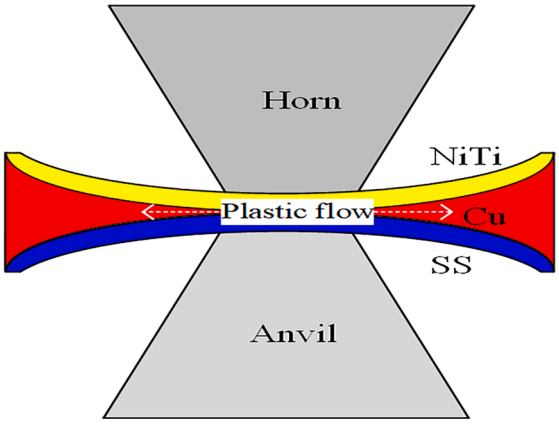

Fig. 6. Schematic of the plastic flow behavior of the Cu interlayer.

has enough bonding density (the level of microbonds at the interface). Therefore, these unbonded zones must be responsible for the low joint strength at a 500 J welding energy input. When the welding energy increased to 750 J, only few voids were detected and microbonds gradually covered the weld interface. Although a small unbonded zone was also detected on the weld interface (indicated by the dashed ellipse in Fig. 5 (b)), the length of the unbonded area accounts for a small proportion of the total length of the weld interface, implying that it would have no significant adverse effect on the joint strength. Small cracks or unbonded zones, which are typical defects under excessive energy conditions (indicated with a dashed white rectangle in Fig. 5 (c)), were found on the NiTi surface and weld interface when the welding energy was increased to 1000 J, causing the deterioration of the joint performance.

When the ultrasonic oscillation was imposed on the materials

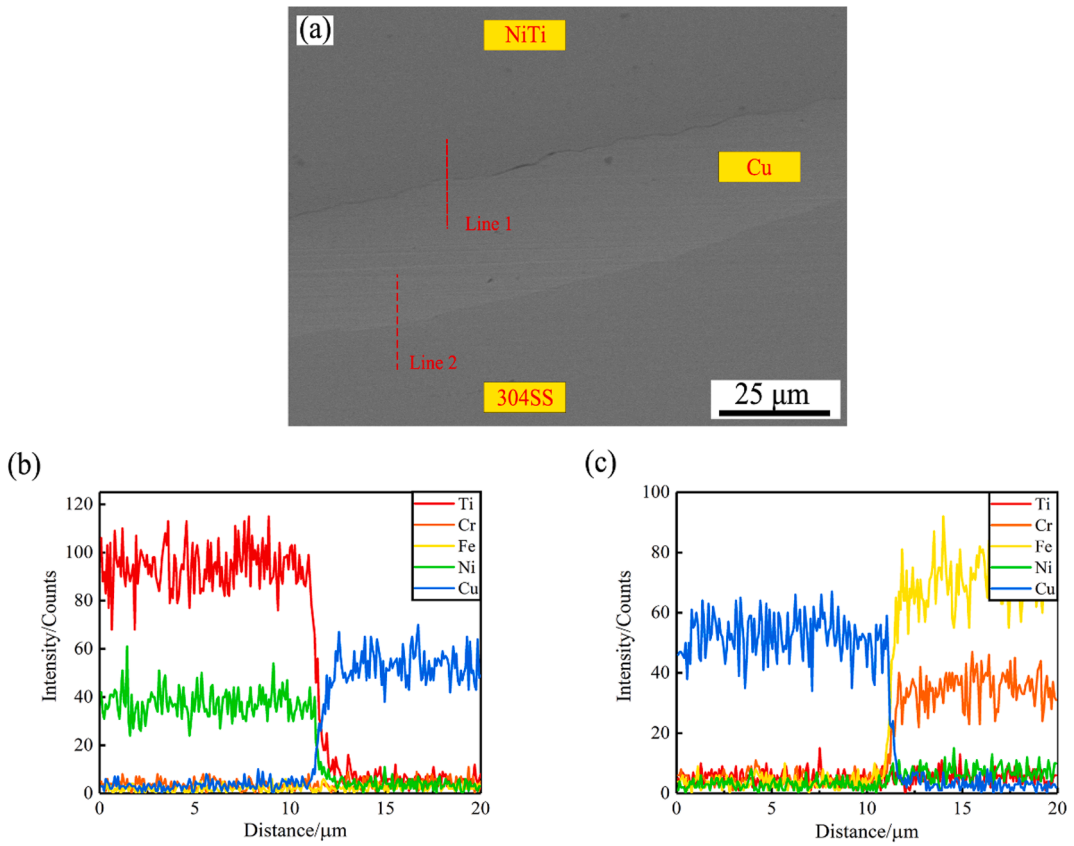

Fig. 7. (a) SEM image of NiTi-Cu-304 SS interface of joints produced with 750 J, (b) EDS line scan results at the NiTi-Cu interface, Line 1, (c) EDS line scan results at the Cu-304 SS interface, Line 2.

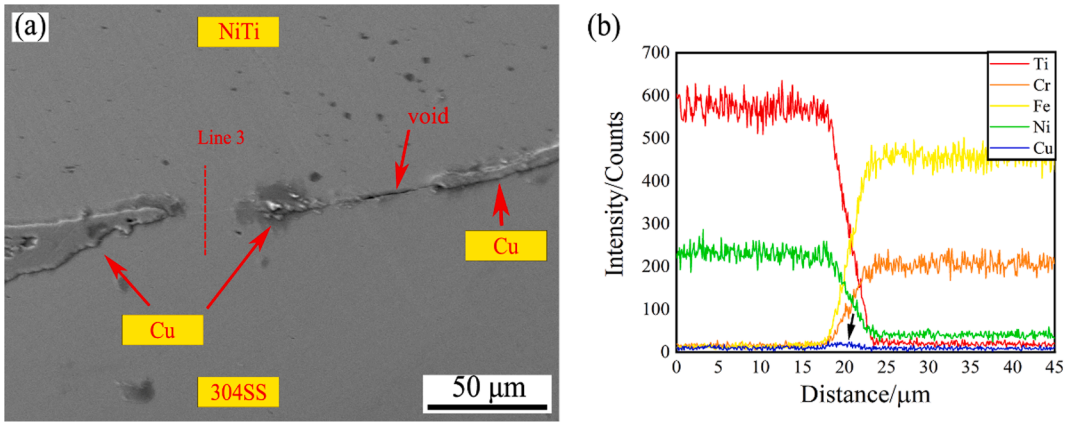

Fig. 8. (a) Typical SEM image of NiTi-304 SS direct contact interface of joints produced with 750 J, (b) EDS line scan results at the NiTi-304 SS interface, Line 3.

through the sonotrode horns, the Cu interlayer was subjected to more severe plastic deformation than NiTi and 304 SS due to its much lower hardness. Clearly, it is seen from Fig. 5 (b) that there are regions of the Cu interlayer with different thickness at the weld interface. The areas under the edges of the sonotrode tips usually show more plastic deformation than other areas, arising from the non-uniform contact pressure under the sonotrode horns. Therefore, the Cu interlayer would flow to other areas, which would significantly modify the thickness of the Cu interlayer. This plastic flow behavior of the Cu interlayer is illustrated by Fig. 6. As shown in the Fig. 6, the Cu interlayer under the knurls of the sonotrode tip will flow. As a result, two typical types of interfaces, including the NiTi-304 SS interface and the NiTi-Cu-304 SS interface, formed after the USW process. In order to detect the interlayer reaction and the possible formation of IMCs at the weld interfaces, high-magnification SEM image with EDS line scanning was taken at the interfaces of the joint produced with energy input of 750 J, as shown in Fig. 7 and Fig. 8.

It could be seen that both NiTi/Cu and Cu/SS weld interfaces were tightly bonded with no visible gaps and IMCs layers. To confirm the chemical composition and the potential phases formation during USW process, EDS line scanning was carried out at the interfaces of the NiTi-Cu-304 SS joint, as shown in Fig. 7 (b)-(c). The results indicate that the distribution of elements at the interface varies greatly in a narrow region of joint produced at 750 J, suggesting that no IMCs were formed at the interfaces. Therefore, it can be concluded that no new reaction phases were formed between the NiTi/Cu and Cu/SS interfaces on the micro

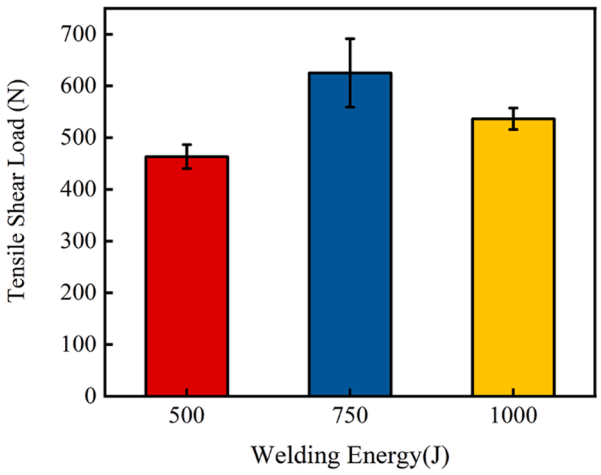

Fig. 9. Average tensile lap-shear load of the USWed joints as a function of welding energy ranging from 500 to 1000 J.

scale during USW.

For the NiTi-SS interface, it can be seen from Fig. 8 (a) that the severe plastic deformation behavior of the Cu interlayer resulted in different thicknesses of the Cu interlayer at the interface. The void was found near the NiTi-SS interface, which might be attributed to the short duration of the USW process, leading to Cu interlayer failed to fill the void after the USW process. Besides, the EDS scanning of the NiTi-SS interface in Fig. 8 (b) has a similar tendency with that of the NiTi-Cu-SS interface. The atomic diffusion layer of NiTi-SS made at 750 J was very short, which was related to the insufficient diffusion between NiTi and 304 SS due to the short welding duration and low interfacial temperature. As pointed out by Zhang et al. [36], the effective diffusion distance of Cu element into the NiTi and SS is beyond 5 μm during hot isostatic pressing (HIP) diffusion bonding. Compared with HIP, the thermal cycle duration in USW is significantly shorter, corresponding to a lower peak termperature and permance time at high temperatures. As a result, long-distance atomic diffusion would be difficult to occur. The arrow depicted in Fig. 8 (b) shows the atomic diffusion of the Cu interlayer, which revealed that a small amount of Cu diffused into the BM, forming a thin diffusion layer at the weld interface. Also, no obvious IMCs were found at the NiTi-SS interface under the 750 J energy input. It should be noted that the atomic diffusion distance of the NiTi-SS interface is slightly longer than that of the NiTi-Cu-SS interface, which can be attributed to the higher contact stress under the edges of the sonotrode tips. Therefore, more plastic deformation, combined with higher temperature, occurred at this area, contributing to the atomic diffusion among NiTi, Cu and SS. As a result, a thicker atomic diffusion layer formed.

3.4. Joints performance and failure analysis

The lap-shear test results of the welded joints, as a function of the welding nergy input, are shown in Fig. 9. It can be seen that the welding energy has a significant effect on the admissible lap-shear loads of the joints. The average tensile shear load increased when the welding energy increased from 500 to 750 J, at which the maximum value of 690 N was achieved, then the ultimate lap-shear load decreased with further increase of welding energy to 1000 J.

At the low welding energy input of 500 J, there was a small microbonded zone under the sonotrode tip ridges due to the limited heat generation, material softening and plastic deformation of the BM. The low energy input prevented the bonding zone from expanding throughout the whole weld zone. The joint performance was improved significantly with increasing energy input as the bonded areas spread throughout the whole interface, which was attributed to the enhanced heat generation, material softening and plastic deformation of the Cu interlayer. The maximum lap-shear load was higher than that of USWed NiTi-NiTi joint with Cu interlayer, reported by Zhang et al. [26]. It is believed that the higher lap-shear load obtained in the present study was related to the lower hardness of 304 SS compared to the NiTi alloy under the same welding conditions. As such, the 304 SS experienced a higher degree of softening during welding, and more rubbing with severe plastic deformation was achieved at the weld interface, contributing to more microbonds and resultant better joint performance.

To reveal the deformation and fracture mechanism of the USWed dissimilar NiTi/SS joints, fracture surfaces of the joint produced at 750 J were examined by the SEM, and the typical images are shown in Fig. 10. The images of the entire fracture surfaces on the NiTi and 304 SS sides are shown in Fig. 10 (a)-(b), respectively. It could be seen that most of Cu was attached to the 304 SS side of the fracture surface, while only a small amount of Cu, located in and around the weld spots, was stuck on the NiTi side, suggesting that the failure occurred mainly at the NiTi/Cu interface. The Cu interlayer got fractured under the peaks of the sonotrode tip during USW process due to the high stress concentration at the edges of the weld spots. In order to obtain more details about the fracture morphology and elemental distribution, EDS analysis was conducted on both sides of the fracture surface. From Fig. 10 (c)-(d), it can be observed that both NiTi and 304 SS sides consisted of two regions: welded spots and scratched zones. Distinct cracks could be observed at the center and edges of the welded spots, indicating that significant deformation occurred under the peaks of the sonotrode tip. Fig. 10 (e)-(f) show higher magnification images of the corresponding areas, indicated with green dashed boxes in Fig. 10 (c)-(d). EDS analysis conducted on the region as indicated in Fig. 10 (e) shows that the region contained (in at. %) 49.5 Ti, 47.9 Ni and 1.74 Cu, suggesting that the Cu foil was stuck to the NiTi matrix. EDS analysis of the region as indicated in Fig. 10 (f) had a composition of (in at. %) 99.3 Cu. Therefore, it can be inferred that very little Cu diffused to the NiTi side, while NiTi diffusion to the Cu interlayer was negligible, which is in agreement with the work by Zhang et al. [27], indicating that the lap-shear strength outside the welded spots at the NiTi/Cu interface is relative weak. Since NiTi is harder than Cu, the Cu interlayer experienced more severe shear plastic deformation induced by the sonotrode tip than the NiTi side during the USW process, causing the Cu foil to get stuck on NiTi alloy. This significant difference in hardness between NiTi and Cu also induced cracking under the sonotrode tip.

In order to further observe the fracture morphology and elemental distribution on the NiTi and SS fracture surfaces, the selected areas were further magnified by SEM, as shown in Fig. 10 (g)-(i). In Fig. 10 (g), typical stepped laminar structures with river marks can be observed, suggesting that the welded spots on the NiTi failed in brittle mode. The EDS analysis of the upper ridges showed that this region had a composition of (in at. %) 48.3 Ni, 46.2 Ti, 2.52 Fe and 1.95 Cu, implying that no obvious atomic diffusion occurred in this region. Furthermore, EDS analysis of the two regions indicated by the yellow box in Fig. 10 (i) and the lower zone in Fig. 10 (g) shows a composition consistent with that of 304 SS on the fracture surface of NiTi side, suggesting that the 304 SS matrix along with Cu interlayer was pulled out to adhere to the NiTi matrix, leading to a higher lap-shear load. However, EDS line scan results in Fig. 10 (j) reveals that only partial 304 SS matrix and Cu interlayer were transferred to the NiTi side under the USW process, and cracks were also observed on the NiTi matrix. Fig. 10 (h) shows the higher magnification of zone “h” in Fig. 10 (f). Fine dimples were clearly observed, indicating the ductile fracture mode in the Cu area. This region has a composition of 96.2 Cu, 2.28 Fe and 0.80 Cr (at. %). As reported by Zhang et al. [26], the Cu interlayer could compensate for the thermal stress generated during the USW process and enhance the friction coefficient on the faying interface. Therefore, it can be inferred that the Cu interlayer could improve the performance of the NiTi/304 SS dissimilar joints. Meanwhile, the tearing zones revealed that the edges of welded spots were the weak regions, which were subjected to high stress concentration under the sonotrode tips, leading to the fracture of joints

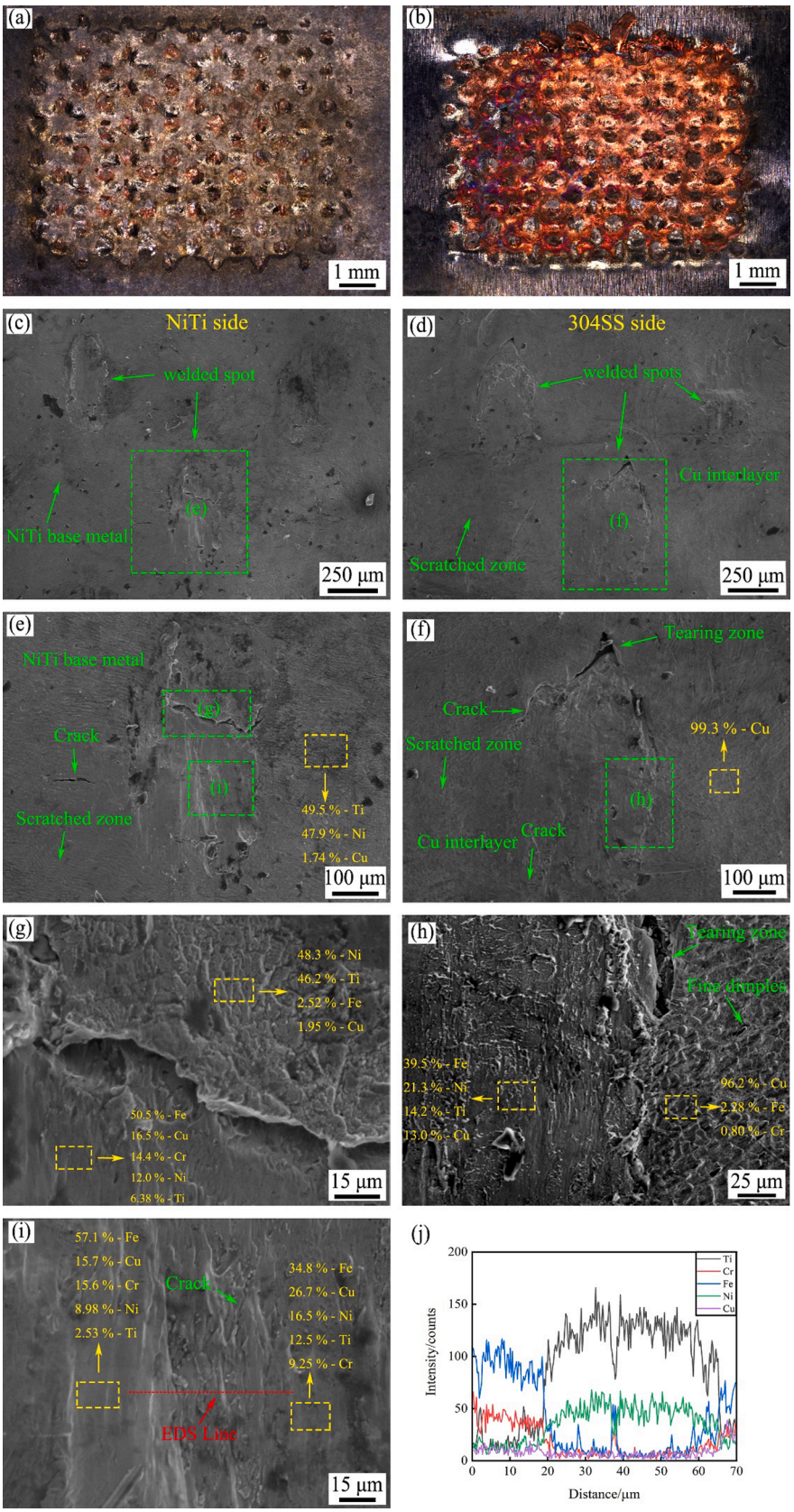

Fig. 10. Typical images of tensile lap-shear fracture surfaces of NiTi/304 SS dissimilar joint produced at a energy of 750 J: (a) overall view on the NiTi side, (b) overall view on the 304 SS side, (c) magnified view on the NiTi surface, (d) magnified view on the 304 SS surface, (e) and (f) at a higher magnification of box in (c) and (d), (g), (h) and (i) at a further higher magnification of box in (e) and (f), (j) chemical composition across the weld spot, the EDS line scan position is indicated in (i).

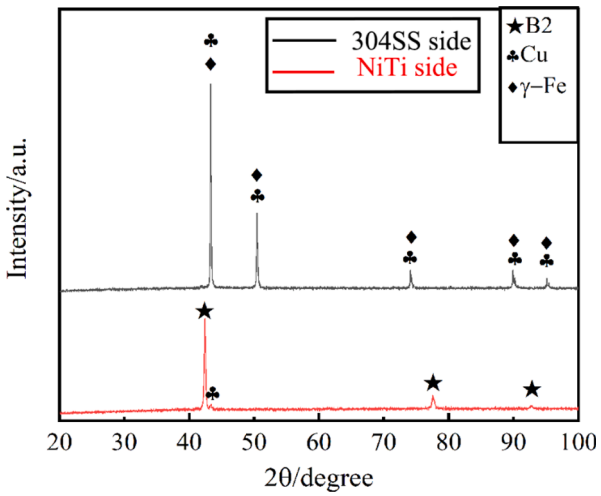

Fig. 11. XRD patterns obtained from both fracture surfaces of NiTi side and 304 SS side.

during the lap-shear tensile tests.

Based on the interface microstructure and fracture surface analysis, it can be concluded that microbonds formed due the friction between the sheets under the sonotrode tip, resulting in the 304 SS matrix being pulled out to adhere to the NiTi side. During the USW process, the sonotrode tip exerted normal force and shear force on the sheets. Friction was then induced between the faying surfaces due to the ultrasonic vibration and then microbonding occurred under the peaks of the sonotrode tip because of high contact stress in these areas. As the welding proceeded, thinning and rupture of Cu interlayer would occur due to the friction and severe plastic deformation. Therefore, the NiTi and 304 SS would be in contact directly under the weld spots owing to the breakage of Cu foil. Eventually, atomic diffusion would be enhanced because of the increase in vacancy concentration and temperature induced by the high strain rate during the USW process [37], resulting in a portion of the 304 SS and Cu interlayer stuck on the NiTi side.

To further characterize the microstructure and confirm the observations above, XRD analysis was conducted on the NiTi and 304 SS fracture surfaces, respectively, and the results are shown in Fig. 11. From the XRD patterns, it can be noticed that a large amount of B2 austenite, along with fewer peaks of Cu were detected on the fracture surface of the NiTi side, which is consistent with the electron microscopy images. The fracture surface of 304 SS only consisted of γ-Fe phase and Cu phase due to the limited miscibility between Cu and Fe. It is worth noting that identical FCC crystal structure and similar lattice constants would contribute to the strong overlap of γ-Fe phase and Cu phase [38]. No IMCs were detected on both fracture surfaces, which is consistent with the EDS analysis above.

4. Conclusions

NiTi alloy was joined to 304 SS with Cu interlayer using various welding energy inputs by USW process. The weld interface microstructure, lap-shear load, and fracture mechanisms were analyzed. The following conclusions can be drawn:

1. The interfacial peak temperature gradually increased from 263.6 °C to 314.5 °C and 387.4 °C with the increasing energy input of 500, 750 and1000 J. With increasing welding energy input from 500 to 1000 J, more friction heat was generated at the specimen surface and weld interface, leading to a higher degree of surface oxidation and plastic deformation. A welding energy of 750 J produced joints with well-bonded weld interfaces.
2. The weld interface of the joints shows two typical types of NiTi-Cu-304 SS interface and NiTi-304 SS interface due to the plastic flow behavior of the Cu interlayer. EDS and XRD analysis indicated that no IMCs were found at both interfaces of the dissimilar joints under different energy inputs.
3. The lap-shear load of the joints increased with welding energy up to 750 J, at which an average peak load of ~690 N was obtained. The peak load decreased with further increase in energy input.
4. All joints obtained under different energy inputs showed interfacial failure mode. Most of the Cu interlayer remained attached to the 304 SS side of the fracture surface. A small amount of Cu was stuck to the NiTi side under the edges of sonotrode tips.

Declaration of Competing Interest

The authors declare that they have no known competing financial interests or personal relationships that could have appeared to influence the work reported in this paper.

Acknowledgements

Supporting for the National Natural Science Foundation of China (No. U1933129), Natural Science Foundation of Tianjin Science and Technology Correspondent Project (No. 18JCQNJC04100, No. 19JCZDJC39000 and No. 19YFFCYS00090). JPO acknowledges the Fundação para a Ciência e Tecnologia (FCT) for its support via the project UID/00667/2020 (UNIDEMI).

References

[1] Z. Zeng, B.Q. Cong, J.P. Oliveira, W.C. Ke, N. Schell, B. Peng, Z.W. Qi, F.G. Ge, W. Zhang, S.S. Ao, Wire and arc additive manufacturing of a Ni-rich NiTi shape memory alloy: Microstructure and mechanical properties, Addit. Manuf. 32 (2020) 101051, https://doi.org/10.1016/j.addma.2020.101051.
[2] J.P. Oliveira, R.M. Miranda, F.M. Braz Fernandes, Welding and joining of NiTi shape memory alloys: A review, Prog. Mater. Sci. 88 (2017) 412–466, https://doi.org/10.1016/j.pmatsci.2017.04.008.
[3] Q. Zheng, X. Zhuang, J. Hu, Z. Zhao, Materials characterization formability of the heat-assisted fine-blanking process for 304 stainless steel plates, Mater. Charact. 166 (2020) 110452, https://doi.org/10.1016/j.matchar.2020.110452.
[4] S. Asadi, T. Saeid, A. Valanezhad, I. Watanabe, J. Khalil-Allafi, The effect of annealing temperature on microstructure and mechanical properties of dissimilar laser welded superelastic NiTi to austenitic stainless steels orthodontic archwires, J. Mech. Behav. Biomed. Mater. 109 (2020) 103818, https://doi.org/10.1016/j.jmbbm.2020.103818.
[5] S. Asadi, T. Saeid, A. Valanezhad, I. Watanabe, J. Khalil-alla, Effects of Ni powder addition on microstructure and mechanical properties of NiTi to AISI 304 stainless steel archwire dissimilar laser welds, J. Manuf. Process. 55 (2020) 13–21, https://doi.org/10.1016/j.jmapro.2020.03.041.
[6] G. Fox, R. Hahnlen, M.J. Dapino, Fusion welding of nickel–titanium and 304 stainless steel tubes : Part II : tungsten inert gas welding, J. Intell. Mater. Syst. Struct. 24 (2012) 962–972, https://doi.org/10.1177/1045389X12461076.
[7] R. Hahnlen, G. Fox, M.J. Dapino, Fusion welding of nickel – titanium and 304 stainless steel tubes : Part I : laser welding, J. Intell. Mater. Syst. Struct. 24 (2012) 945–961, https://doi.org/10.1177/1045389X12461075.
[8] G.R. Mirshekari, A. Saatchi, A. Kermanpur, S.K. Sadrnezhaad, Laser welding of NiTi shape memory alloy : Comparison of the similar and dissimilar joints to AISI 304 stainless steel, Opt. Laser Technol. 54 (2013) 151–158, https://doi.org/10.1016/j.optlastec.2013.05.014.
[9] M.G. Li, D.Q. Sun, X.M. Qiu, J.B. Liu, K. Miao, W.C. Wu, Effects of silver based filler metals on microstructure and properties of laser brazed joints between TiNi shape memory alloy and stainless steel, Sci. Technol. Weld. Joining 12 (2) (2013) 183–188, https://doi.org/10.1179/174329307X164418.
[10] H.M. Li, D.Q. Sun, X.L. Cai, P. Dong, W.Q. Wang, Laser welding of TiNi shape memory alloy and stainless steel using Ni interlayer, Mater. Des. 39 (2012) 285–293, https://doi.org/10.1016/j.matdes.2012.02.031.
[11] Y. Chen, S. Sun, T. Zhang, X. Zhou, S. Li, Effects of post-weld heat treatment on the microstructure and mechanical properties of laser-welded NiTi/304SS joint with Ni filler, Mater. Sci. Eng., A 771 (2020) 138545, https://doi.org/10.1016/j.msea.2019.138545.
[12] X.-L. Gao, X.-Q. Wang, J. Liu, L.-K. Li, A novel laser welding method for the reliable joining of NiTi/301SS, Mater. Lett. 268 (2020) 127573, https://doi.org/10.1016/j.matlet.2020.127573.
[13] H. Li, D. Sun, X. Cai, P. Dong, X. Gu, Laser welding of TiNi shape memory alloy and stainless steel using Co filler metal, Opt. Laser Technol. 45 (2013) 453–460, https://doi.org/10.1016/j.optlastec.2012.06.010.

[14] H. Li, D. Sun, X. Gu, P. Dong, Z. Lv, Effects of the thickness of Cu filler metal on the microstructure and properties of laser-welded TiNi alloy and stainless steel joint, Mater. Des. 50 (2013) 342–350, https://doi.org/10.1016/j.matdes.2013.03.014.
[15] C.H. Ng, E.S.H. Mok, H.C. Man, Effect of Ta interlayer on laser welding of NiTi to AISI 316L stainless steel, J. Mater. Process. Technol. 226 (2015) 69–77, https://doi.org/10.1016/j.jmatprotec.2015.06.039.
[16] J. Pouquet, R.M. Miranda, L. Quintino, S. Williams, Dissimilar laser welding of NiTi to stainless steel, Int. J. Adv. Manuf. Technol. 61 (1–4) (2012) 205–212, https://doi.org/10.1007/s00170-011-3694-7.
[17] M.J.C. Oliveira, R.H.F. Melo, T.M. Maciel, A.C.J. De, Microstructural evaluation and mechanical behaviour of dissimilar niti- stainless steel joints welded by micro gas tungsten arc welding, Mater. Chem. Phys. 224 (2019) 137–147, https://doi.org/10.1016/j.matchemphys.2018.12.013.
[18] P. Vondrous, Plasma ARC welding of NiTi and 304 steel, in: 23rd DAAAM international symposium on intelligent manufacturing and automation, vol. 2, 2012, pp. 1039–1042.
[19] Q. Li, Y. Zhu, J. Guo, Microstructure and mechanical properties of resistance-welded NiTi/stainless steel joints, J. Mater. Process. Technol. 249 (2017) 538–548, https://doi.org/10.1016/j.jmatprotec.2017.07.001.
[20] S. Belyaev, V. Rubanik, N. Resnina, V. Rubanik, O. Rubanik, V. Borisov, Phase transitions : A multinational martensitic transformation and physical properties of 'steel–TiNi' bimetal composite, produced by explosion welding, Phase Trans. 83 (4) (2010) 276–283, https://doi.org/10.1080/01411591003656757.
[21] S. Fukumoto, T. Inoue, S. Mizuno, K. Okita, T. Tomita, A. Yamamoto, Friction welding of TiNi alloy to stainless steel using Ni interlayer, Sci. Technol. Weld. Joining 15 (2) (2013) 124–130, https://doi.org/10.1179/136217109X12577814486692.
[22] Q. Li, Y. Zhu, Impact butt welding of NiTi and stainless steel- An examination of impact speed e ff ect, J. Mater. Process. Tech. 255 (2018) 434–442, https://doi.org/10.1016/j.jmatprotec.2017.12.046.
[23] H. Huang, J. Chen, J.H. Cheng, Y.C. Lim, X.H. Hu, Z.L. Feng, X. Sun, Surface engineering to enhance heat generation and joint strength in dissimilar materials AZ31 and DP590 ultrasonic welding, Int. J. Adv. Manuf. Technol. 111 (11–12) (2020) 3095–3109, https://doi.org/10.1007/s00170-020-06341-3.
[24] C.J. Li, S.S. Ao, J.P. Oliveira, M.P. Cheng, Z. Zeng, H.J. Cui, Z. Luo, Ultrasonic spot welded NiTi joints using an aluminum interlayer: Microstructure and mechanical behavior, J. Manuf. Process. 56 (2020) 1201–1210, https://doi.org/10.1016/j.jmapro.2020.05.043.
[25] C.J. Li, S.S. Ao, J.P. Oliveira, Z. Zeng, H.J. Cui, Z. Luo, Effects of post-weld heat treatment on the phase transformation and mechanical behavior of NiTi ultrasonic spot welded joints with Al interlayer, J. Manuf. Sci. Eng. 142 (10) (2020), 101006, https://doi.org/10.1115/1.4048002.
[26] W. Zhang, S.S. Ao, J.P. Oliveira, Z. Zeng, Y. Huang, Z. Luo, Microstructural characterization and mechanical behavior of NiTi shape memory alloys ultrasonic joints using Cu interlayer, Materials 11 (2018) 1–14, https://doi.org/10.3390/ma11101830.
[27] W. Zhang, S.S. Ao, J.P. Oliveira, C. Li, Z. Zeng, A. Wang, Z. Luo, On the metallurgical joining mechanism during ultrasonic spot welding of NiTi using a Cu interlayer, Scr. Mater. 178 (2020) 414–417, https://doi.org/10.1016/j.scriptamat.2019.12.012.
[28] S.S. Ao, W. Zhang, C.J. Li, J.P. Oliveira, Z. Zeng, Z. Luo, Variable-parameter NiTi ultrasonic spot welding with Cu interlayer, Mater. Manuf. Process. 36 (5) (2021) 599–607, https://doi.org/10.1080/10426914.2020.1843676.
[29] A. Mahmud, Z. Wu, J. Zhang, Y. Liu, H. Yang, Surface oxidation of NiTi and its effects on thermal and mechanical properties, Intermetallics 103 (2018) 52–62, https://doi.org/10.1016/j.intermet.2018.09.013.
[30] O. Cissé, O. Savadogo, M. Wu, L'H. Yahia, Effect of surface treatment of NiTi alloy on its corrosion behavior in Hanks' solution, J. Biomed. Mater. Res. 61 (3) (2002) 339–345, https://doi.org/10.1002/jbm.10114.
[31] M.P. Satpathy, B. Patel, S.K. Sahoo, Exploration of bonding phenomenon and microstructural characterization during high-power ultrasonic spot welding of aluminum to steel sheets with copper interlayer, Ain. Shams Eng. J. 10 (4) (2019) 811–819, https://doi.org/10.1016/j.asej.2019.07.007.
[32] M. Shakil, N.H. Tariq, M. Ahmad, M.A. Choudhary, J.I. Akhter, S.S. Babu, Effect of ultrasonic welding parameters on microstructure and mechanical properties of dissimilar joints, Mater. Des. 55 (2014) 263–273, https://doi.org/10.1016/j.matdes.2013.09.074.
[33] S.S. Lee, T.H. Kim, S.J. Hu, W.W. Cai, J.A. Abell, J.J. Li, Characterization of joint quality in ultrasonic welding of battery tabs, J. Manuf. Sci. Eng. 135 (2) (2013), 021004, https://doi.org/10.1115/1.4023364.
[34] S. Elangovan, S. Semeer, K. Prakasan, Temperature and stress distribution in ultrasonic metal welding-An FEA-based study, J. Mater. Process. Technol. 209 (3) (2009) 1143–1150, https://doi.org/10.1016/j.jmatprotec.2008.03.032.
[35] D. Bakavos, P.B. Prangnell, Mechanisms of joint and microstructure formation in high power ultrasonic spot welding 6111 aluminium automotive sheet, Mater. Sci. Eng., A 527 (23) (2010) 6320–6334, https://doi.org/10.1016/j.msea.2010.06.038.
[36] J. Zhang, D. Xie, Q. Li, C. Jiang, Q. Li, Effect of holding time on the microstructure and strength of tungsten/steel joints by HIP diffusion bonded using a Cu interlayer, Mater. Lett. 261 (2020) 1–4, https://doi.org/10.1016/j.matlet.2019.126875.
[37] I. Gunduz, T. Ando, E. Shattuck, P. Wong, C. Doumanidis, Enhanced diffusion and phase transformations during ultrasonic welding of zinc and aluminum, Scr. Mater. 52 (9) (2005) 939–943, https://doi.org/10.1016/j.scriptamat.2004.12.015.
[38] C.F. Tey, X. Tan, S.L. Sing, W.Y. Yeong, Additive manufacturing of multiple materials by selective laser melting : Ti- alloy to stainless steel via a Cu-alloy interlayer, Addit. Manuf. 31 (2020) 1–16, https://doi.org/10.1016/j.addma.2019.100970.